Laser Frequency Stabilization to Optical and Atomic References

Matthias Metternich

Bachelorarbeit in Physik
angefertigt im Institut für Angewandte Physik

vorgelegt der
Mathematisch-Naturwissenschaftlichen Fakultät
der
Rheinischen Friedrich-Wilhelms-Universität
Bonn

August 2024

Ich versichere, dass ich diese Arbeit selbstständig verfasst und keine anderen als die angegebenen Quellen und Hilfsmittel benutzt sowie die Zitate kenntlich gemacht habe.

Bonn, 14.08.2024 M. Metternich

Datum Unterschrift

1. Gutachter: Prof. Dr. Sebastian Hofferberth
2. Gutachter: Prof. Dr. Daqing Wang

Contents

CHAPTER 1

Introduction

Since the first demonstrations of laser operation in 1960 [1] lasers have become an integrated part of atomic physics experiments [2]. Lasers with stable and tunable frequencies are used for many applications including addressing of atomic transitions for instance for laser cooling [3] or for creation of Rydberg atoms [4]. The frequency of a laser is influenced by many different parameters, such as diode temperature, air pressure, and humidity as well as vibrations and laser diode current noise [5]. It is impossible to keep the laser stable in frequency, by trying to suppress external noise factors. However, the laser can be actively stabilized in a feedback loop where changes of the laser frequency are registered and used to provide a feedback signal back to the laser.

The goal of this thesis is to construct feedback loops for stabilizing the frequency of two lasers and to characterize the performance of the frequency stabilization. While most of the lasers used in the Nonlinear Quantum Optics group are commercial, the lasers used for this project are self-built narrow linewidth interference filter lasers. These two lasers were recently refurbished to a wavelength of 780 nm [6] which corresponds to the D_2-line of Rubidium [7]. Frequency stabilization of these two self-built lasers is the first step in making them ready for application in an experiment with ultracold rubidium where a stabilized laser frequency is needed. This work also serves as a process description on how self-built interference filter lasers can be stabilized.

In order to perform laser frequency stabilization, a highly stable reference is required that makes it possible to detect laser frequency drifts and fluctuations. In this project two different types of references are used to perform frequency stabilization, which are an optical and an atomic reference. There are other options that can also be used as a reference for laser frequency stabilization, such as an optical cavity [8] as in the Pound-Drever-Hall method [9].

The thesis is structured as follows. In the following section the setup of the self-built interference filter laser is discussed. Chapter 2 shows how an error signal can be generated from an atomic and an optical reference. The idea is to use a hyperfine transition in Rubidium as an optical reference for the stabilization by using the change of absorption rate in a Rubidium cell while the laser beam propagates through it. A frequency change of the laser output corresponds to a change in absorption rate which is detectable with a photodiode. This stabilized laser is used as a reference for a beatnote stabilization of a second laser.

Chapter 3 shows how the error signal can be used as feedback to stabilize the laser. A network analyzer is used to measure transfer functions which leads to a better understanding of how the feedback loops react to different disturbing signals in the frequency domain. Other parts were added to the feedback loops and optimized such as a PID controller. In addition, special care was taken to remove high-frequency noise up to roughly 1 MHz. Finally, the long term stability of the feedback loops is analyzed and characterized, since the stabilization should last over a longer time span for application in a cold atom lab.

1.1 Interference filter lasers

The used lasers are two external cavity interference filter lasers. This type of laser was first presented in 1981 [10]. In this thesis single-ended external cavity lasers were used, with the diode representing one end of the cavity. This is realized by using a laser diode with a reflective coating on its backside.

The laser design is illustrated in Figure 1.1. The setup involves a laser diode, three lenses, an interference filter, and an outcoupling mirror mounted on a piezo stack. The laser diode is supplied with current by a current controller. The first lense collimates the laser diode output before it is passing the interference filter. The interference filter determines the achievable frequency range of the laser due to its rotation angle and leads to a narrow transmission peak [11]. After that the transmitted beam is focused to the outcoupling mirror which partly outcouples the laser light and partly provides optical feedback to the laser diode. The voltage given to the piezo element adjusts the distance between the second lense and the mirror. Since the second lense is fixed with screws as well as the others, the mirror is shifted due to this modulation, which results in a change in the length of the cavity. This change of the resonator length can be used to tune the laser frequency. At the end the third lense collimates the outcoupled laser beam. The laser is mounted in a protective housing. More information about the setup of this lasers as well as their characteristics can be found in Hannah Buss bachelor thesis [6]. Also included is a temperature control which can be used to adjust the laser frequency but has a very slow response.

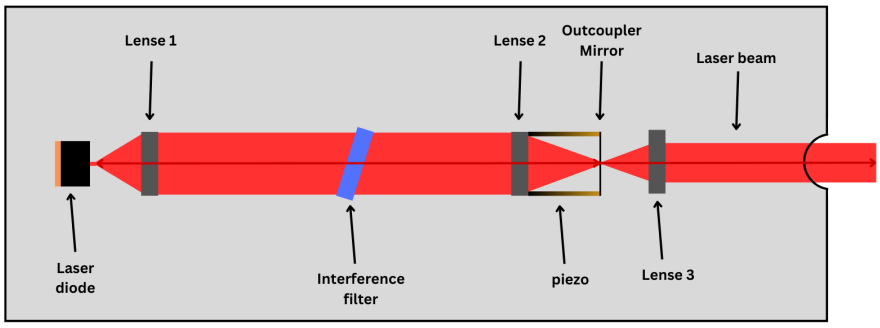

Figure 1.1: Design of the interference filter lasers used in this thesis. The laser diode output is collimated by the first lense before passing the interference filter. After that it is focused on the outcoupling mirror before it is collimated again by the third lense. The piezo element, which is a ring piezo connecting the second lense and the outcoupling mirror, can be used to adjust the resonator length.

CHAPTER 2

Error signal generation

For laser frequency stabilization with a feedback loop, a reference is needed. The error signal is created by comparing the laser frequency to the reference. In this chapter two different approaches of creating an error signal are being presented. Section 2.1 shows the error signal created with an atomic reference where absorption spectroscopy is used to translate a frequency change into a beam intensity change which can be detected with a photodiode. Section 2.2 shows how to create an error signal in dependence of the beatnote frequency between two lasers. The basic requirement for both error signals is that a frequency change results in a voltage change of the error signal, and that the sign of this voltage change depends on the sign of the frequency change. Optimizations for a better feedback loop can then follow, for example by adding a control algorithm.

2.1 Creation of an error signal from an atomic reference

The error signal creation from an atomic reference is done by using Doppler free saturated absorption spectroscopy [12]. The basic concept is that a change in frequency results in a large enough change of the absorption rate which is detectable with a photodiode. There are different types of error signals that can be created from an atomic reference through spectroscopy such as side of fringe and top of fringe error signals [5]. Here a side of fringe error signal was generated and used for the frequency stabilization. A fringe is the absorption around an atomic resonance. While a side fringe was used for this purpose, a stabilized laser, which is used to drive atomic transitions in an experiment, must be precisely tuned to the atomic resonance. Subsection 2.1.1 shows the setup for the error signal generation while the created error signal is shown and discussed in subsection 2.1.2.

2.1.1 Saturated absorption spectroscopy

A hyperfine structure transition of the D_2-line in Rubidium is used to create the error signal. In order to resolve hyperfine levels, classical absorption spectroscopy is not enough because it is doppler broadened. A different approach is therefore necessary.

Doppler free saturated absorption spectroscopy can be used to reach the needed resolution for this error signal generation. The idea is to overlap two counter propagating laser beams with the same wavelength. The two beams differ in intensity with one being called pump beam and the weaker one called probe

beam. A two level system is assumed where the pump beam equalizes the population between the ground and the excited state. While the laser frequency is not in resonance with the atomic transition for atoms that do not move along the laser axis, both beams address atoms with a different sign of velocity which makes the result the same as with Doppler broadened absorption spectroscopy. However, while the laser frequency is in resonance with the atomic transition for atoms that do not move along the laser axis both beams are addressing the same atoms [13]. The excitations lead to less absorption of the probe beam and therefore to peaks within the absorption spectrum which are called lamb dips.

How this is realized is shown in Figure 2.1. A half-waveplate (HWP) and a polarizing beam splitter (PBS) are used to control how much laser light is used for the spectroscopy. The laser beam then propagates through the rubidium cell, a filter and a quarter-waveplate (QWP) before it is retro-reflected and overlapped with itself. The filter ensures that the probe beam intensity is significantly lower than the pump beam intensity. The QWP is used to make sure the pump beam is being transmitted at the PBS and therefore hitting the photodiode. With this setup small frequency changes are detectable with the photodiode.

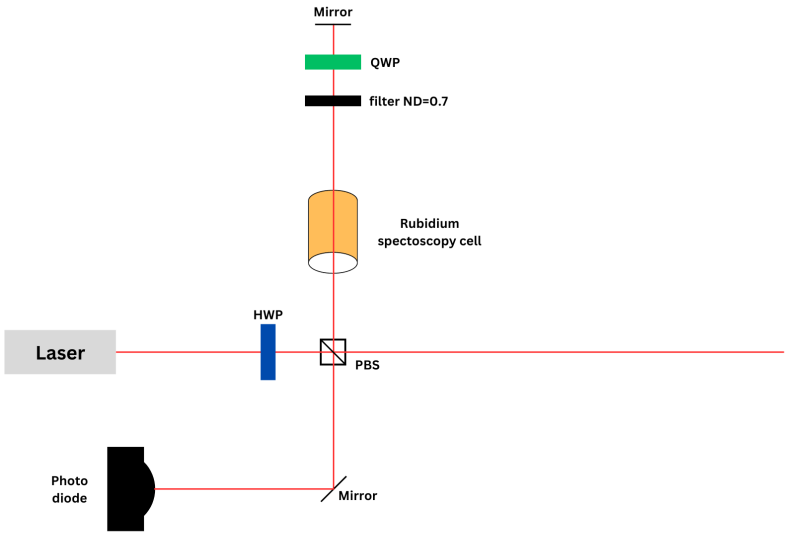

Figure 2.1: Doppler free saturated absorption spectroscopy setup. A part of the laser beam is used for Doppler free saturated spectroscopy where it goes through a rubidium spectroscopy cell, gets attenuated and reflected and goes through the cell again before hitting a photodiode. The beam initially transmitted through the PBS can be used for experiments with the stabilized laser.

2.1.2 Side of fringe error signal

Now that the hyperfine structures can be resolved, an error signal can be generated. Rubidium has two naturally occurring isotopes which are ^{85}Rb, whose mole fraction is 0.7217(2) and ^{87}Rb whose mole fraction is 0.2783(2) [14] (p.760). For this error signal generation the D_2-line of ^{87}Rb whose level scheme is shown in Figure 2.2 is used. For this stabilization a fringe side of a lamb dip of the $F = 2 \rightarrow F'$

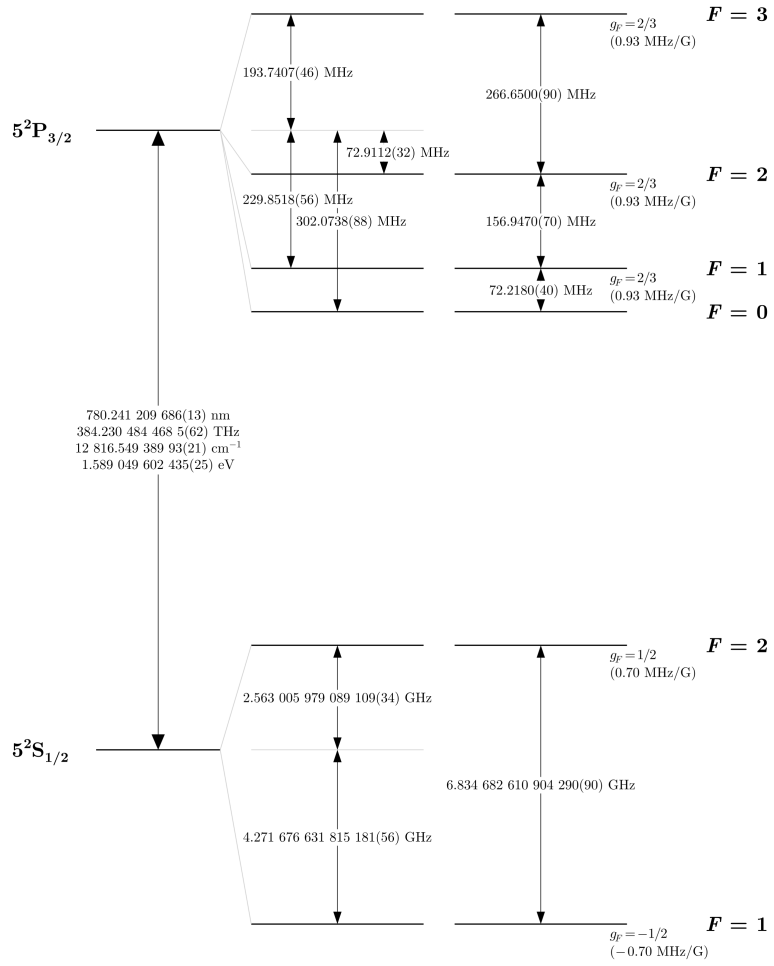

Figure 2.2: Level scheme for the D_2-line of ^{87}Rb including hyperfine structure transitions, taken from [7].

transition is chosen.

Due to the selection rule $\Delta F = 0, \pm 1$ three lamb dips should be observable. The measured spectrum is shown in Figure 2.3 which was done by applying an alternating voltage ramp signal to the piezo element of the laser which results in a linear frequency scan and measuring the photodiode output with an oscilloscope. For the frequency stabilization the side of fringe of the $F = 2 \rightarrow F = 2'$ transition is used due to its high slope which is marked in orange in Figure 2.3. A zero crossing can be created by mixing the photodiode signal that is shown in Figure 2.3 with an offset. This results in a positive voltage of the error signal for frequency changes in one direction and a negative voltage for frequency changes in the other direction which can be then used as feedback to the laser directly or though a control algorithm.

The two plots in Figure 2.3 show the measurement for different settings of the HWP which results in different total amounts of light used for each measurement, while the ratio between the probe and pump beam stayed constant. The less light is used for the spectroscopy, the lower the slope of the error

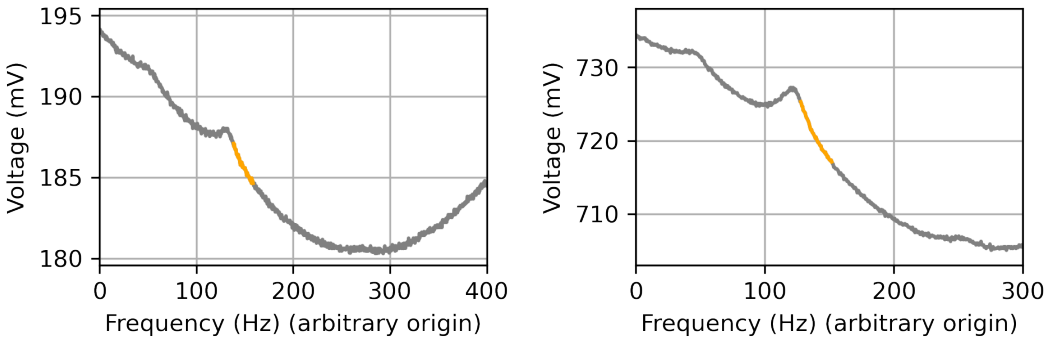

Figure 2.3: Doppler free saturated spectroscopy of the $F = 2 \rightarrow F'$ transitions of the D_2-line of ^{87}Rb with two different amounts of laser beam intensity used. The slope which will be used as the fringe side error signal is shown in orange.

signal and the resolution of the lamb dips. The slope of the orange curve part in the left plot is roughly 0.12 mV/MHz and in the right plot roughly 0.34 mV/MHz. Nevertheless the HWP setting from the left plot was used in the following, as the goal is to achieve a frequency stabilization with as little laser light intensity as possible, so there is more laser light intensity which can be used for other applications as well as for the other frequency stabilization where this laser frequency is used as a reference.

2.2 Creation of an error signal from an optical reference

In this section, it is described how the error signal is generated using a delay line box. It follows the principle as it was first done in 1999 [15]. The error signal is generated by using a delay line to create an interference signal which depends on the frequency of the beat signal between the two laser beams. The laser to which the feedback will be given is denoted the slave laser. In contrast to that the other laser is denoted the master laser which is the one stabilized to the atomic reference. The stabilization is designed such that the frequency of the slave laser follows the frequency of the master laser with a certain offset. Subsection 2.2.1 shows the setup of the delay line box as well as the functions of the individual components for the error signal generation. Subsection 2.2.2 shows the measured error signals and compares them with the theoretical expectations.

2.2.1 Setup of a delay line box

The setup of the delay line box is shown in Figure 2.4. At first two laser beams with the same polarization have to overlap and hit a photodiode. For this purpose a fast photodiode[1] which has a bandwidth up to 6 GHz is used. After that the signal of the photodiode is used as input into the delay line box.

To get the voltage on the photodiode it is necessary to consider the intensity of the two fields at the photodiode. The result is shown in equation 2.4 where ω_1 and ω_2 are the laser frequencies.

[1] Hamamatsu G4176-03

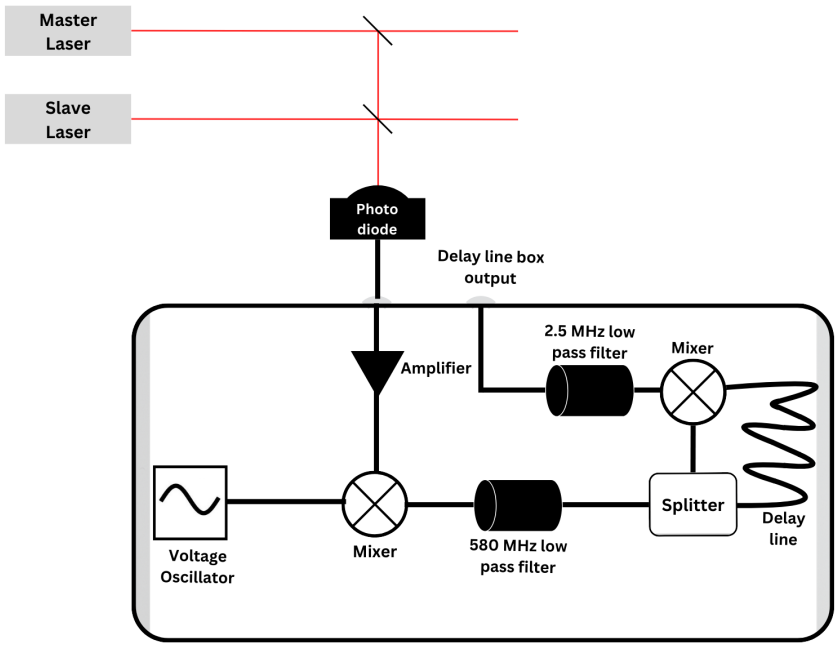

Figure 2.4: Setup of error signal creation with a delay line box. Two lasers are being overlapped and aligned onto a photodiode. The photodiode signal is given as input to the delay line box where it gets amplified. After that the signal is mixed with a voltage controlled oscillator signal which frequency can be tuned with an external voltage. The mixer output runs through a 580 MHz low pass filter before it is split. After delaying one arm, the two arms are mixed back together. At the end the mixer output runs through a 2.5 MHz lowpass filter.

$$I_{PD} \propto (\cos(\omega_1 t) + \cos(\omega_2 t))^2 \tag{2.1}$$
$$\propto \cos^2(\omega_1 t) + \cos^2(\omega_2 t) + 2\cos(\omega_1 t)\cos(\omega_2 t) \tag{2.2}$$
$$\propto \frac{1}{2}(2 + \cos(2\omega_1 t) + \cos(2\omega_2 t) + 2\frac{1}{2}\cos((\omega_1 + \omega_2)t) + \cos((\omega_1 - \omega_2)t) \tag{2.3}$$
$$\propto 1 + \frac{1}{2}(\cos(2\omega_1 t) + \cos(2\omega_2 t)) + \cos((\omega_1 + \omega_2)t) + \cos((\omega_1 - \omega_2)t) \tag{2.4}$$

The photodiode is AC-coupled which filters out the DC term in equation 2.4. Of the AC terms, only the $\cos((\omega_1 - \omega_2)t)$ term can possibly be detected, as the other frequencies are in the hundreds of THz so they are not detectable by a photodiode. Therefore the delay line box input is $\cos(\omega_b t)$ with the beatnote frequency $\omega_b = \omega_1 - \omega_2$.

Inside the delayline box the signal is amplified as shown in Figure 2.4. After the amplification, tbe beatnote signal is mixed with the signal from an external voltage controlled oscillator. The frequency of the external voltage controlled oscillator is denoted by ω_O. The resulting signal is shown in equation 2.5 with $\omega_\pm = \omega_b \pm \omega_O$.

$$\cos(\omega_b) \cdot \cos(\omega_O) = \frac{1}{2}(\cos(\omega_b + \omega_O)\cos(\omega_b - \omega_O)) \propto \cos(\omega_+) + \cos(\omega_-) \tag{2.5}$$

The oscillator frequency can be controlled by an external voltage. The lowest frequency that can be reached with the used voltage controlled oscillator[2] is around 800 MHz. So independent of the chosen oscillator frequency and the beatnote frequency, the 580 MHz low pass filter eliminates the $\cos(\omega_+)$ term. The signal is then divided in two parts where one part has to go through a delay line before they both are recombined at a mixer. The time delay between the two signals can be described by

$$\Delta t = \frac{l}{c} \tag{2.6}$$

where l is the length and c the signal speed in the delay line cable. The mixer output can then be described by

$$\cos(\omega_- t) \cdot \cos\left(\omega_-(t + \frac{l}{c})\right) = \frac{1}{2}\left(\cos\left(\omega_- t + \omega_-(t + \frac{l}{c})\right)\cos\left(\omega_- t - \omega_-(t + \frac{l}{c})\right)\right) \tag{2.7}$$

$$= \frac{1}{2}\left(\cos(2\omega_- t + \omega_- \frac{l}{c}) + \cos(\omega_- \frac{l}{c})\right). \tag{2.8}$$

The 2.5 MHz lowpass filter eliminates the time oscillating term in equation 2.8. After this lowpass filter the delay line box gives a time independent cosine output which just depends on ω_-, l and c. A zero crossing of this cosine can now be used as a locking point. A change of ω_b and therefore ω_- leads to an increasing or decreasing output voltage which can be then given as feedback to the slave laser.

2.2.2 Error signals for different delay line lengths

The error signal was measured by giving a triangular ramp signal to the piezo modulation of the laser the same way as it was done in subsection 2.1.2. The measured error signals are shown in Figure A.1 for different delay lines. Four different delay lines have been used:

- Delay line 1: (58.0 ± 1.0) cm
- Delay line 2: (98.5 ± 1.5) cm
- Delay line 3: (197.5 ± 3.5) cm
- Delay line 4: (397.5 ± 4.5) cm

The expected cosine function can be seen as well as some irregular disturbances for $\omega_- \approx 0$. This behaviour can be explained with equation 2.8 as the time-dependent term is not eliminated for $\omega_- \approx 0$. It can be seen that the error signal slope at a zero crossing gets higher for longer delay lines. It would be theoretically expected that error signal slope and delay line length are proportional to each other which

[2] Mini-Circuits ZX95-2150VW-S+

follows from equation 2.8. It also shows that the error signal frequency gets higher for longer delay lines.

Every zero crossing in the same direction can be used as a locking point. The direction to be used depends on whether the frequency of the slave laser is higher or lower than that of the master laser. The distance between two zero crossings of the same direction, which corresponds to one cosine period, represents the capture range of a locking point. Theoretically, it would be expected that the capture range and delay line length are inversely proportional to each other. To show that the error signals were measured a second time for higher values of ω_- so that the capture range can be extracted for every delay line length. This is shown in Figure 2.5. It can also be seen that the error signal amplitude gets lower for too high ω_- values which is caused by the 580 MHz low pass filter. The linear relation between delay line length and error signal slope as well as the inversely proportional relation between delay line length and error signal capture range are shown in Figure 2.6.

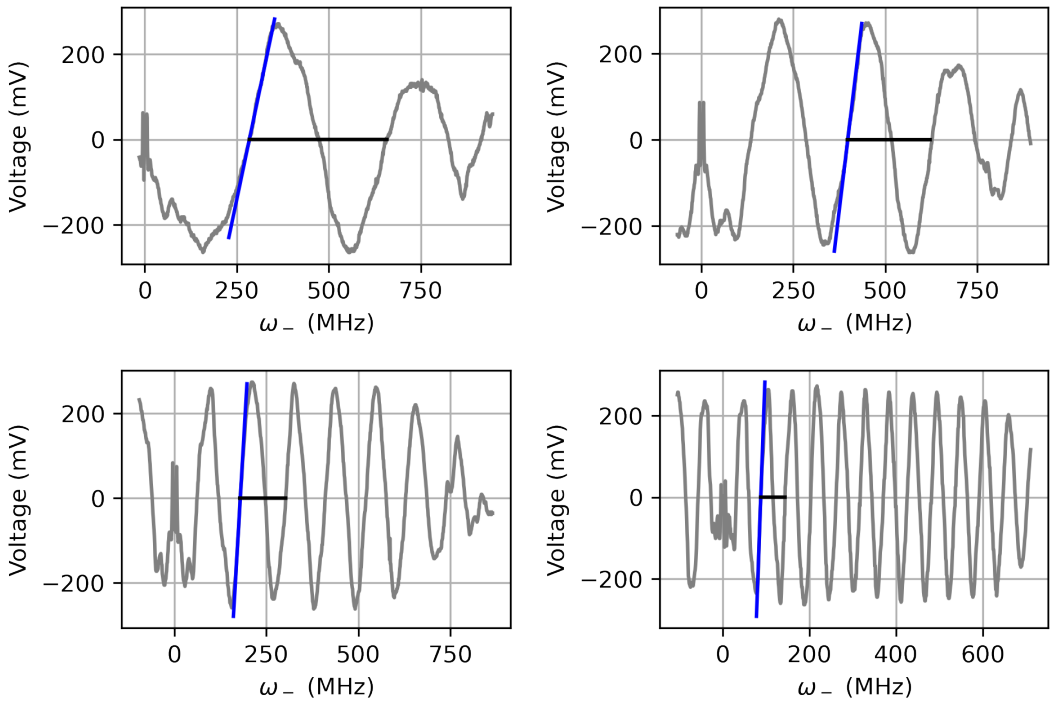

Figure 2.5: Measured error signals for different delay line lengths (top left (l = 58.0 ± 1.0) cm, top right (l = 98.5 ± 1.5) cm, bottom left (l = 197.5 ± 3.5) cm, and bottom right l = (397.5 ± 4.5) cm). The extracted slopes and capture ranges are shown in Table A.1. The slope increases and the capture range decreases for longer delay lines. There is also a decrease in amplitude for high ω_-(= $\omega_b - \omega_O$, see equation 2.5) due to the 580 MHz lowpass filter. The measurement was done by giving a ramp signal to the piezo modulation while simultaneously measuring the beatnote frequency with a spectrum analyzer.

After the laser is locked once the beatnote frequency can be fine adjusted by changing the frequency of the voltage controlled oscillator inside the delay line box. The longest delay line has been chosen to be used due to its large slope and sufficiently large capture range of 56 MHz. In contrast to the atomic reference, the delay line length is a parameter that can be adjusted to change the slope independently of

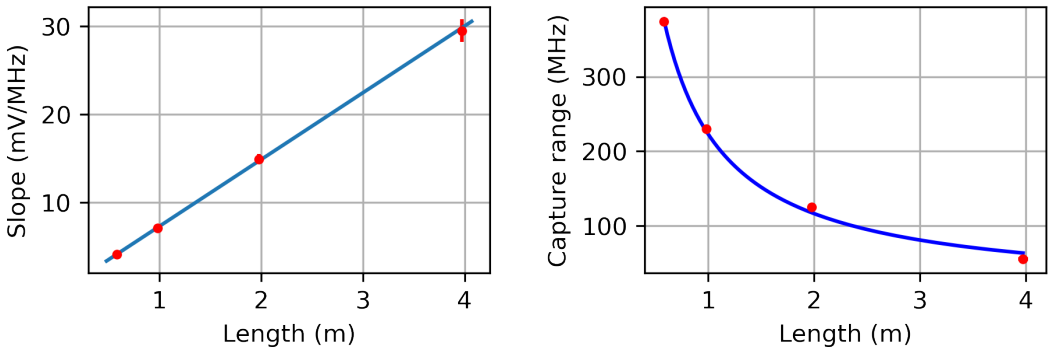

Figure 2.6: Error signal slope and capture range for different delay line lengths. A linear and a $\frac{1}{x}$ fit are used to verify the expected relations. The relations are a consequence of equation 2.8.

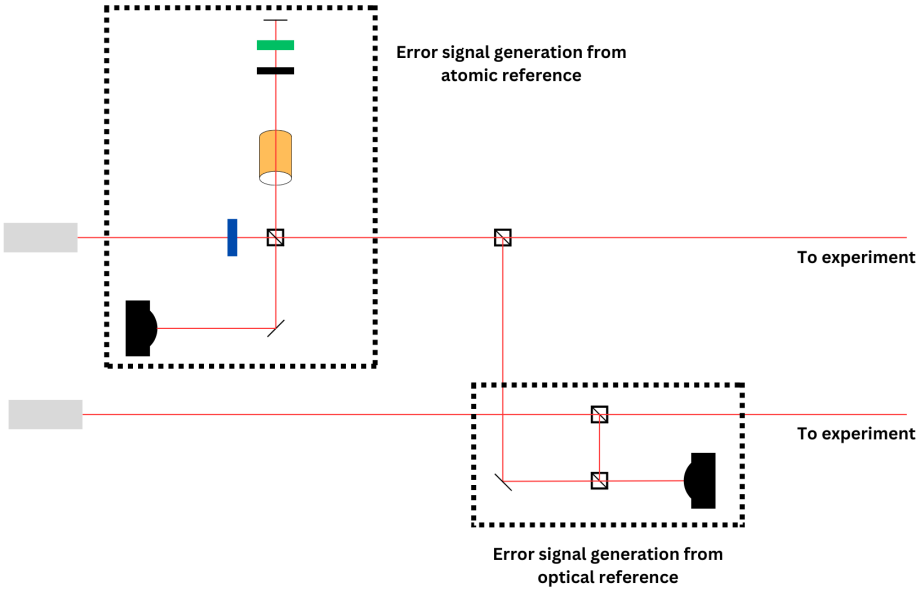

Figure 2.7: Setup of both error signal generations combined.

the amount of laser light used. An error signal slope of 29.5 mV/MHz was achieved with the longest delay line. In comparison to the error signal slope of the master laser which is 0.12 mV/MHz, the error signal slope with the longest delay line is roughly 245 times higher. The whole setup including both error signal generations is shown in Figure 2.7.

However, by implementing a control algorithm, a stabilization can be made with both error signals. An alternative for beatnote stabilization that is often used in the NQO group is a digital phase lock. [16].

CHAPTER 3

Optimizing the feedback loops

The two types of error signals introduced in chapter 2 can now be used to provide feedback to the laser. The error signals can be used as input to the current controller or the piezo element. However, the error signals alone do not lead to effective stabilization. The slope of the error signal from the atomic reference is far too small to make any measurable impact. With the error signal from the optical reference, a measurable impact can be achieved but the stabilization is highly ineffective. To improve the stabilizations, the feedback loops have been extended. A current stealing module is implemented, to be able to stabilize in a higher frequency range. Instead of using the error signals directly as input, a PID controller is included as a control algorithm. A Phase advancer is used to push the servo bump to higher frequencies. At the end of this chapter, the closed loop results of the full feedback loops and the long term stability are analyzed.

A network analyzer is used to characterize the impact of different parts of the feedback loop. The concept of measuring transfer functions with a network analyzer is shown in Figure 3.1. The network analyzer generates one frequency and then looks at the relative change in amplitude and phase of this frequency signal after it runs through the system. The device does this through a set of discrete frequency steps and at each measure the system response. With this data, a Bode plot can be generated that shows the amplitude and the phase of the system response. In this chapter, the response of multiple elements in the feedback loop are characterized and the bode plots for each are discussed.

3.1 Current stealing modulation

The frequency of the laser can be tuned with the current, the temperature, and the piezo element which changes the resonator length. The temperature is not a useful parameter to be applied here because of its slow response which results in a significant time delay in the feedback loop. Therefore, the laser will be stabilized with the laser diode current and the piezo element.

To measure the transfer function of the piezo modulation, a frequency sweep is given from the network analyzer[1] to the piezo element of the laser while the delay line box output is given back to the network analyzer. The setup for this measurement is shown in Figure 3.2. For this purpose, a zero crossing

[1] HP 3589A 10 Hz to 150 MHz Spectrum Network Analyzer

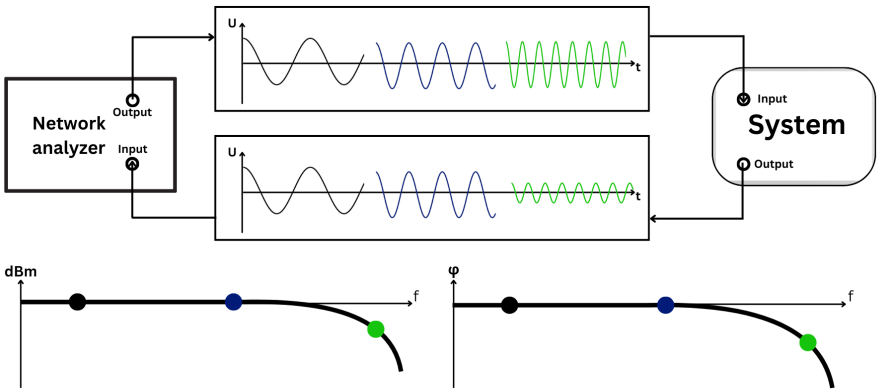

Figure 3.1: Bode Plot generation with a network analyzer. The network analyzer puts a frequency sweep into a system and measures the amplitude and phase of the system response.

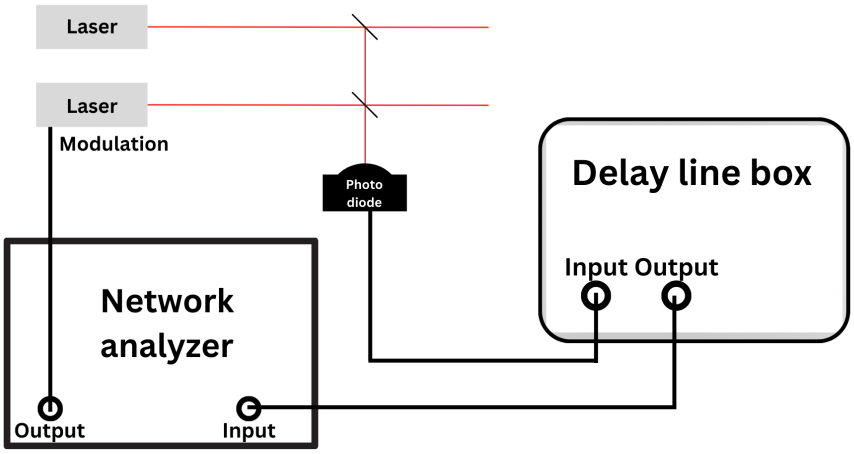

Figure 3.2: Setup for measuring the transfer function of the piezo and current stealing modulation. The output of the network analyzer is used as the modulation source while the delay line box output is given back to the network analyzer. The measurement was taken at a zero crossing of the error signal. The error signals are shown in Figure 2.5.

of the error signal was used and by manually adjusting the frequency of the external oscillator inside the delay line box during the measuring process, it was ensured that the error signal was at the zero crossing during the entire measurement. Otherwise, the beatnote frequency could have drifted so that it would be no longer in the linear range of the error signal, which would have affected the measurement result. Keeping the signal at the zero crossing makes it possible to measure how the piezo modulation affects the laser frequency since there is a linear relation between the delay line box output and the laser frequency change.

Figure 3.3 shows the measurement result for the piezo modulation of both lasers. The piezo element has a very limited bandwidth and drives mechanical resonances in the 10 kHz regime. Even though several resonances can be observed, there is a particularly strong resonance with the opposite phase at 73 kHz for both lasers. This resonance could also be measured with the spectrum analyzer, as shown

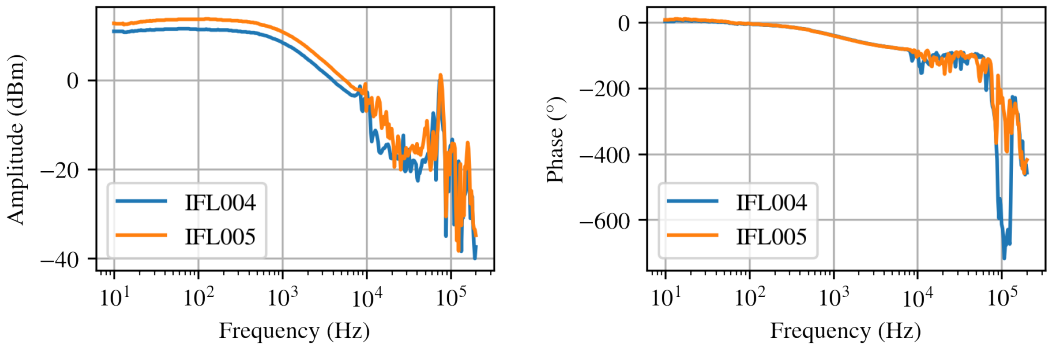

Figure 3.3: Piezo modulation transfer function measured with the network analyzer. The piezo drives mechanical resonances in the 10 kHz regime.

in Figure A.3, by connecting the delay line box error signal to the piezo elements of a laser and a part of the delay line box input to the spectrum analyzer. Those resonances will have to be cut off with an external lowpass filter. Therefore piezo feedback can only be used to compensate for frequency drifts and low-frequency fluctuations up to roughly a few kHz but it is incapable of higher frequency compensation.

To stabilize the lasers at higher frequencies the current is the only parameter that can be utilized. The current is controlled by a ThorLabs ITC 102 current controller. The lasers were built in a way that the signal from the current controller has to pass an LC lowpass filter with roughly 1 kHz bandwidth before going through the laser diode to reduce laser diode current noise caused by the controller. Therefore giving feedback to the current controller is also not an option for high-frequency stabilization. One option to implement a stabilization method for high frequencies is to provide the feedback signal directly to the laser diode through a path with a resistor and a capacitor that bypasses the lowpass filter. The disadvantage of this method is that one has to be careful not to change the current that goes through the laser diode too much in a very short period of time as this can destroy the laser diode. This could happen due to a too strong feedback signal or an electrical shock while plugging in the cable [2] (p.10). A safer way to use high-frequency current modulation is to implement a current stealing path after the lowpass filter where the current stealing rate can be controlled through an external signal. This can be realized with a field-effect transistor (FET) as done in reference [16]. How this is realized in this specific configuration is shown in Figure 3.4. A junction FET (JFET) and a safety diode are implemented after the current controller signal passed the lowpass filter. The modulation signal controls the amount of current that the transistor steals and conducts to ground while the diode ensures that the modulation signal amplitude does not become too high and therefore does not damage the transistor.

The silicon diode strongly limits the amplitude of the current modulation compared with the piezo elements as the piezos have a range of ±15 V. This makes the current stealing incapable of compensating frequency drifts for a longer timescale, as frequency drifts accumulate over time. Therefore the current stealing modulation cannot replace the piezo modulation, instead, the piezo modulation is used to compensate low-frequency fluctuations and frequency drifts, and the current stealing modulation is used to compensate high-frequency fluctuations. The current stealing modulation transfer function, which was measured the same way as the piezo modulation transfer function, is shown in Figure 3.5. The

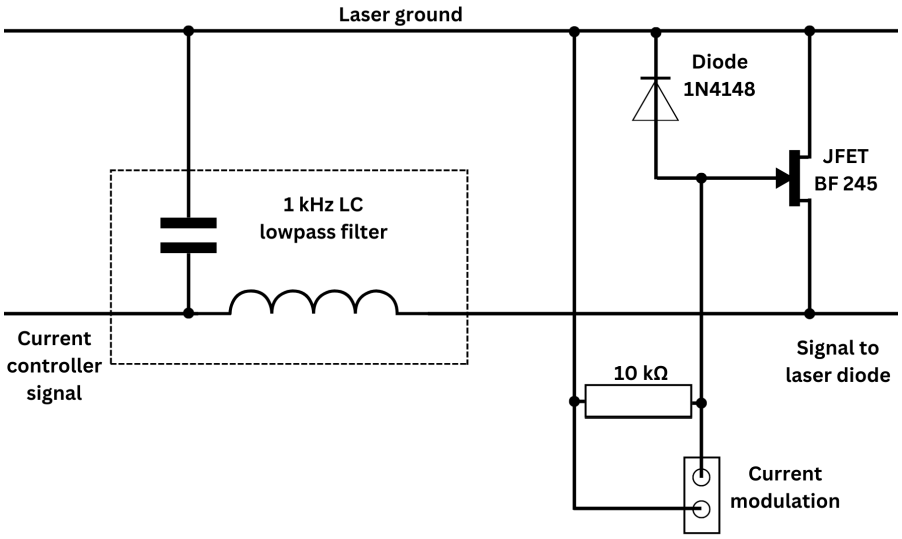

Figure 3.4: Schematic illustration of the implemented current stealing modulation.

transfer functions look very similar for both lasers except for a small deviation for low frequencies which is not relevant because the current modulation will only be used for higher frequencies anyway. Both lasers have a dip in the transfer function at around 1 kHz which corresponds to the cut off frequency of the lowpass filter inside the laser board. The strong amplitude decrease at 2.5 MHz is caused by the lowpass filter inside the delay line box.

The 2.5 MHz lowpass filter does not only cut off the amplitude rapidly but also affects the phase for significantly lower frequencies which is characteristic of a high order lowpass filter. The measured transfer function of this lowpass filter is shown in Figure 3.6. This lowpass filter has been removed so it is not influencing the transfer function measurement of the current stealing modulation anymore. As explained in subsection 2.2.1, the only purpose of this lowpass filter is to cut off the time-dependent oscillating term. However, since a zero crossing can be chosen at such a high ω_- that the frequency of the time-dependent term is too high to be measured with the network analyzer, this lowpass filter is not needed for this measurement.

The measured transfer functions of the current stealing modulation without the 2.5 MHz lowpass filter inside the delay line box are shown in Figure 3.7. Here, the measurement was also taken at different currents provided by the current controller, whereby it is noticeable that the entire amplitude curve shifts on the Y-axis for different currents, but its shape remains the same. The reason is that in the ohmic region, which describes the region where saturation has not yet been reached, the JFET operates like a voltage-controlled resistor [17] (p.100). Therefore, the amount of current conducted to ground is not only dependent on the modulation signal but also on the amount of current provided by the current controller. The consequence is that the frequency stabilization for high-frequency modulation optimized for a current controller output of for example 60 mA does not work just as well for another output such as 45 mA, but has to be optimized again.

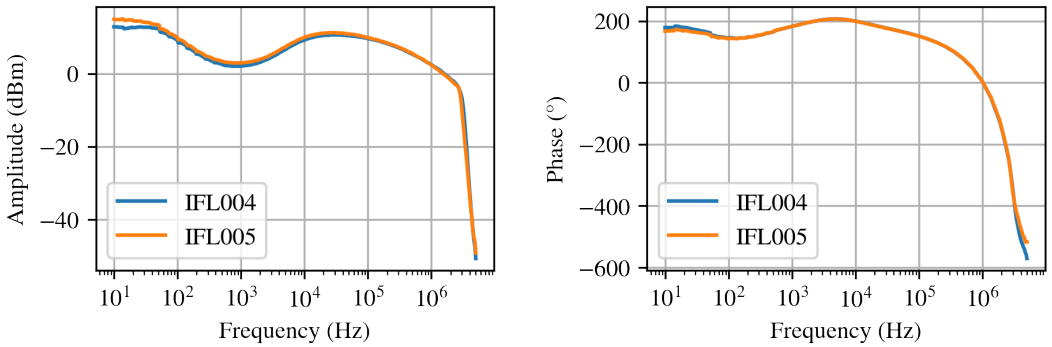

Figure 3.5: Current stealing modulation transfer function measured with the network analyzer. The bandwidth is limited by the 2.5 MHz lowpass filter inside the delay line box. The transfer function without this lowpass filter is shown in Figure 3.7

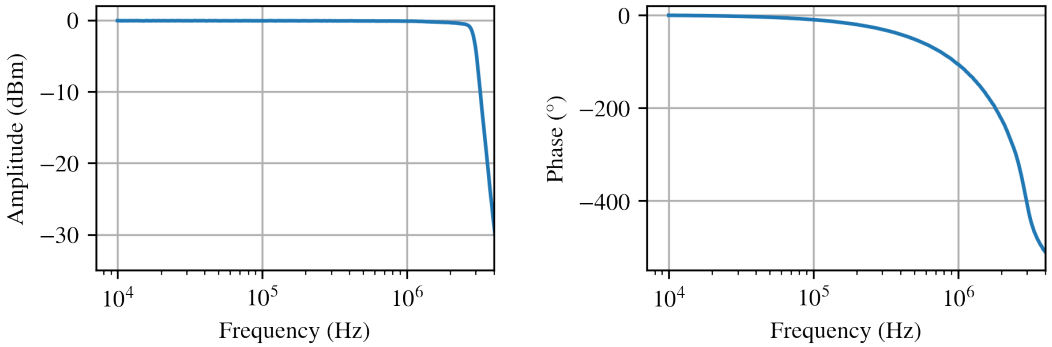

Figure 3.6: Transfer function of the 2.5 MHz lowpass filter inside the delay line box measured with the network analyzer. It is a higher order lowpass filter which results in the rapid decrease of amplitude and the early starting phase decrease.

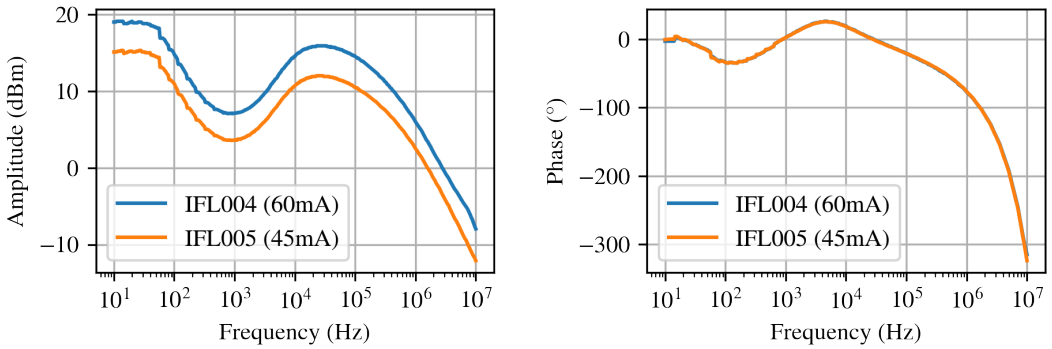

Figure 3.7: Current stealing modulation transfer function measured for different currents with the network analyzer. The 2.5 MHz lowpass has been removed from the delay line box.

3.2 PID controller

Feedback loops can be optimized by using a control algorithm such as a PID controller, loop shaping or optimal control [18]. For these feedback loops a PID controller is chosen which is schematically illustrated in Figure 3.8. It combines two inputs with an error offset.

The second input is not needed for the stabilization but is used here for measuring closed loop transfer functions with the network analyzer. The error offset is necessary for the stabilization to an atomic reference as explained in subsection 2.1.2. The signal is divided into a proportional part, an integral part, and a derivative part. Each part is realised with a circuit including an operational amplifier.

The proportional part is created with an amplifier circuit, the integral part with an integrator and the derivative part with a differentiator. More details about this circuits can be found in reference [17]. Each part has a potentiometer allowing the gain of each to be adjusted separately within a certain range. As shown in [18] (p.804) the PID output is the sum of the outputs of each part of the the controller. It therefore follows for the PID output $u(t)$

$$u(t) = Pe(t) + I \int e(t)dt + D\frac{de(t)}{dt} \tag{3.1}$$

where $e(t)$ is the time-dependent error signal and therefore the PID input. P, I and D are the proportional, integral and derivative gain.

The proportional part multiplies the error signal by a factor which depends on the potentiometer setting. Although the proportional part is an effective tool in suppressing noise for higher frequencies, it suffers from proportional droop [18] (p.794). The proportional part cannot fully compensate DC-values which would lead to frequency drifts of the system over a longer timescale. To prevent this an integrator is used which, through integration, is ideal for eliminating DC-values in the error signal and thereby compensating frequency drifts. The differentiator reacts to the rate of change of the error signal and therefore becomes relevant at higher frequencies while its impact is negligibly small for low frequencies and drifts.

The proportional and differential part were measured both individually and together with the network analyzer, as shown in Figure 3.9. The gains have not been changed between the measurements. The integral part was not directly measured with the network analyzer, since it is not only dependent on the instantaneous signal but also from previous signals, as there is an integration over a certain period of time. However its impact can be visualised using the closed loop transfer function. It can be seen that the different parts of the PID controller all have an intrinsic bandwidth of roughly 1 MHz which is limited by the used operational amplifiers inside the PID controller. The P and PD amplitude curves overlap for up to 10 kHz before the derivative part starts getting relevant. The frequency where the derivative part starts affecting the output can be adjusted by changing the D gain. The measurement also shows a phase lead caused by the derivative part since the differentiator has the characteristics of a phase lead circuit [19] (p.68). As with the amplitude, the phase lead can also be controlled by adjusting the D gain to determine when the derivative part starts to influence the phase of the PD curve. However, the measurement also shows that the phase lead is limited by the bandwidth of the PID controller and can only be realised

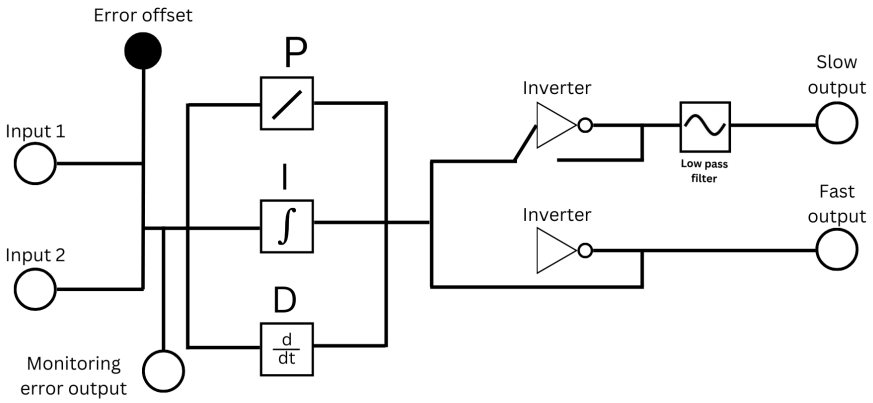

Figure 3.8: Schematic illustration of the used PID controller. Two inputs are combined with an adjustable error offset and then divided into a proportional, integral and derivative part. Every part can be turned on and off with a switch. After that, they are combined again and then split into a fast and a slow output. Both outputs can be inverted and the slow output has an extra lowpass filter included while the fast output bandwidth is limited by the bandwidth of the used operational amplifiers.

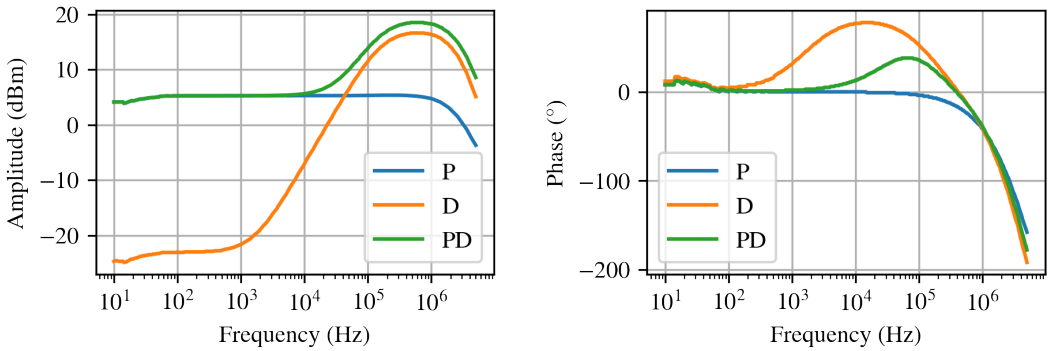

Figure 3.9: Transfer function of the PID controller for the proportional part, the differential part and the proportional and differential part together.

within its bandwidth. To generate a phase lead at frequencies above 1 MHz, the bandwidth of the PID controller must be increased.

As shown in Figure 3.8, the PID controller has two outputs, one contains a lowpass filter and is therefore denoted as slow output, while the other is denoted as fast output. The slow output is connected to the piezo modulation while the fast output is connected to the current stealing modulation, creating a fast and a slow feedback path. The current stealing and piezo modulation have a different sign of impact, as a positive voltage signal leads to a higher laser frequency with the current stealing modulation and a lower laser frequency with the piezo modulation. Since the error signal for the stabilization to the atomic reference is positive for frequencies that are too low and negative for frequencies that are too high as shown in Figure 2.3, the slow output of the PID controller has to be inverted. The error signal to the optical reference on the other side has zero crossings with both signs which is why one output has to be inverted and the other not, but it is irrelevant whether the slow or the fast output is inverted. For the slow

output, a lowpass filter was included to cut off resonances of the piezo elements, as explained in section 3.1. The cut off frequency was chosen to be 1.8 kHz. The fast output is only limited by the bandwidth of the PID controller, as no resonances occur with the current stealing modulation, it does not need to be filtered externally.

3.3 Phase advancer

A characteristic problem of a servo system is that the phase delay resulting from the limit of the bandwidth will lead to a point where the feedback signal approaches a 180° phase lag which leads to positive feedback where the noise is increased rather than suppressed [20] (p.32). In order to shift this servo bump to higher frequencies, a phase advancer is implemented between the fast output of the PID controller and the current stealing modulation. An existing lead lag filter was used for this purpose as shown in Figure 3.10(a). Also integrated in this filter is a capacitor which is utilised as a DC-Block to avoid frequency drift compensation with the current stealing modulation as explained in section 3.1.

The creation of the phase lead is done in principle the same way as in reference [16]. The overall resistance of a circuit with a parallel resistor and capacitor determines how much voltage decreases across a resistor connected in series with it which is also the output voltage. Since the parallel circuit of resistor and capacitor form a voltage divider, a lower total resistance of the parallel circuit leads to a higher amplitude of the output. The total resistance of the parallel circuit R_p can be written by the capacitive resistance as

$$R_p = \frac{R}{1 + 2\pi f C R}. \tag{3.2}$$

Since the capacitive resistance is frequency-dependent, it can be used to generate an increase in the amplitude of the output signal in a certain frequency range, resulting in a phase lead. How a phase advance filter produces a shift of the servo bump to higher frequencies is illustrated in figure 3.10(b). The phase lead shifts the point at which the whole loop reaches 180° phase lag to higher frequencies.

The transfer function of the phase advancer was measured with the network analyzer and is shown in Figure 3.11. The capacitor that is used to block DC signals leads to a strong attenuation of the signal for low frequencies as those should be primarily compensated through the slow feedback path. The cut off frequency here is lower than with the slow feedback path, so that there is no gap in the frequency domain where neither of the two feedback paths works. The resistors and capacitors were adjusted in a way that the phase advance is at its highest between 1 MHz and 10 MHz. This was chosen because as shown in Figure 3.7 and Figure 3.9, the phase lag of 180° of the whole fast feedback path would be located in this frequency span.

The 2.5 MHz lowpass filter inside the delay line box which was already removed for a measurement in section 3.1 will now be removed completely because of the caused phase lag which is shown in Figure 3.6. The lowpass filter would lead to a shift of the servo bump to lower frequencies and therefore to the opposite of what the phase advancer is supposed to achieve. Since the lowpass filter only has the purpose to filter out the time-dependent oscillation inside the delay line box, this will not cause a problem as these

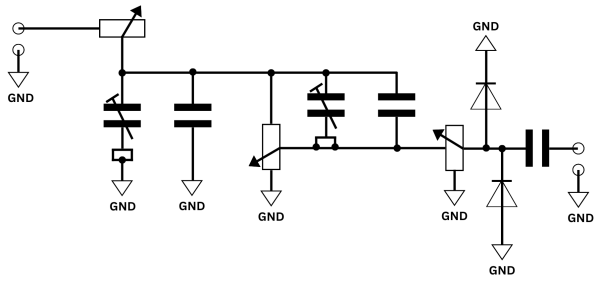

(a) Used circuit for phase advancing. This circuit can be used as a phase lead or a phase lag filter depending on how the capacitors and resistors are set. The last capacitor is used as a DC-Block to prevent the compensation of frequency drifts with the fast feedback path.

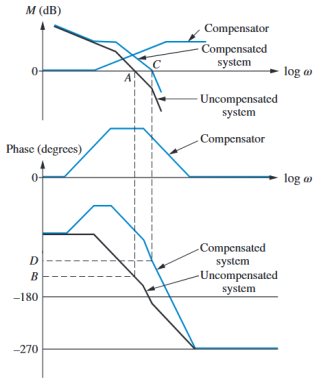

(b) Visualization of phase lead compensation. Figure taken from [21] (p.624).

Figure 3.10: Phase advancer.

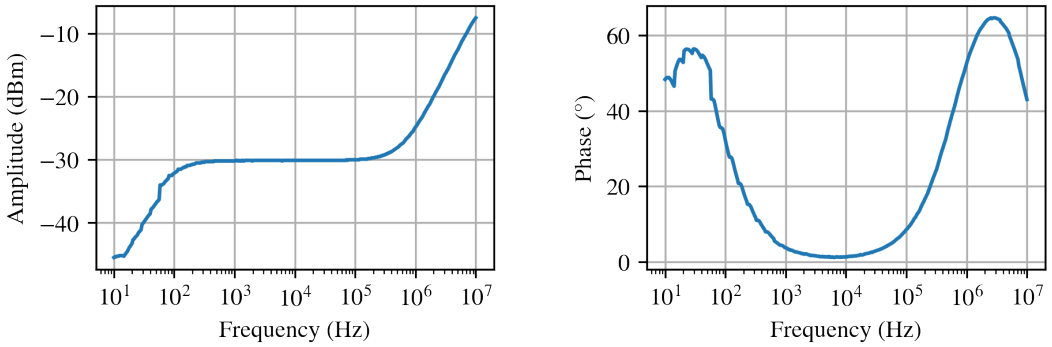

Figure 3.11: Transfer function of the phase advancer measured with the network analyzer.

oscillations at the zero crossings of the error signal are so high in frequency that they are far outside the bandwidth of the PID controller and therefore do not affect the stabilization.

3.4 Closed loop transfer functions

In order to achieve the best possible frequency stabilization, the optimal PID parameters have to be found. The PID controller has a monitoring error output after the two input signals and the error offset are mixed as shown in Figure 3.8. This monitoring output is used to measure the closed loop error signal with the network analyzer. The advantage of this output is that it gives an opportunity to measure the error signal in a closed loop without influencing the measurement result through the process of measuring.

The slope of the error signal generated by the delay line box is so large that the ranges of the

potentiometers for the P, I and D gain were not wide enough for a working stabilization. This problem was solved by significantly attenuating the slow output as this prevents the piezo modulation from overshooting. The frequency stabilization to the atomic reference does not require an attenuation of the slow output since its error signal slope is much lower as described in subsection 2.2.2.

The idea is now to measure the closed loop transfer function while changing the PID parameters to stabilize as good as possible in the frequency domain. This means that the feedback loop has to be optimized in a way that it can suppress noise with a bandwidth as high as possible and also as strong as possible for frequencies within this bandwidth. To measure the impact of the closed loop in this frequency domain, the network analyzer is used to give a frequency sweep into the closed loop while measuring the response of the stabilization through the monitoring output of the PID controller. The frequency sweep of the network analyzer is therefore an external disturbing signal and it is measured how effective the closed loop can eliminate this disturbance. By comparison of the open loop and closed loop measurement it can be determined where in the frequency domain the disturbance is compensated and where it is enhanced. The open loop measurement differs from the closed loop measurement in the sense that the feedback is not fed back to the lasers. This makes it possible to measure how the frequency sweep without feedback affects the monitoring error output, which can be used as a reference as to whether the closed loop can compensate for the disturbance or not.

The frequency sweep from the network analyzer can be applied to the closed loop by using the second input of the PID controller. For the beatnote stabilization the network analyzer signal can alternatively be applied to the current stealing modulation of the master laser. Figure 3.12 shows the open loop and closed loop transfer function as well as the difference between those two methods for the beatnote stabilization. The open loop measurement shows how the respective modulation affects the monitoring error output of the PID controller. Relevant is the difference between open loop and closed loop as this shows the quality of compensation in the frequency domain. This difference is denoted as compensation curve here. The sign of the compensation curve shows whether noise is increased or suppressed. The comparison of the difference between open and closed loop transfer functions for both possibilities to measure those is shown in Figure 3.12. Both methods, apart from some noise, are leading to the same compensation curve. Therefore, it does not make a difference on what point of the closed loop the disturbing signal is included. Both methods are capable of measuring the effects of the closed loop. In the following, all measurements were taken by using the second input of the PID controller.

In order to illustrate the influence of the respective parts of the PID controller, the closed loop transfer function was measured for stabilizations with P only, with PI and PID. As frequency drifts can happen with only the proportional part, the error signal had to be kept at a zero crossing by manually changing the external oscillator frequency inside the delay line box during the measurement process. The closed loop transfer functions determined compensation curves are shown in Figure 3.13. A certain noise suppression can already be achieved with the proportional part until the servo bump occurs between 1 MHz and 10 MHz. The compensation curve of the proportional part also reaches a local high between 1 kHz and 10 kHz which is caused by the servo bump of the slow path. However the fast feedback path compensation can suppress the slow path servo bump. Activating the integrator now leads to a significant improvement at low frequencies. The integrator gain drops by approximately 20 dBm per decade until it overlaps with the curve of the P part for high frequencies. The derivative part leads to a slightly better stabilization between 100 kHz and 1 MHz but at the cost of a much higher amplitude of the servo bump.

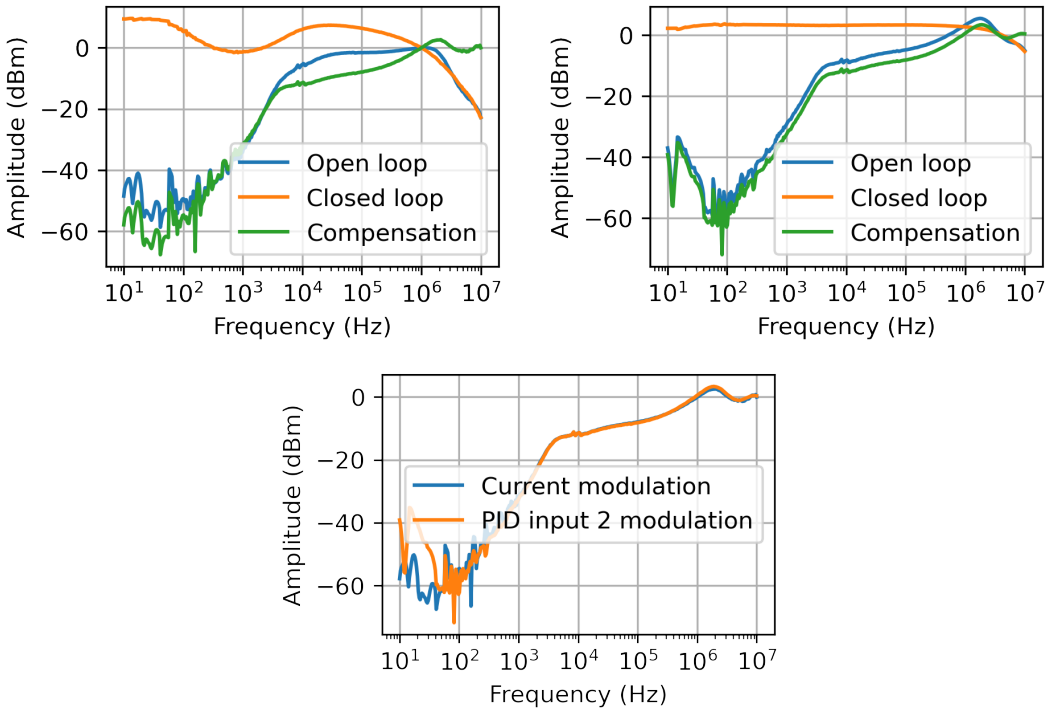

Figure 3.12: Creating a compensation curve as the difference of the closed loop and open loop transfer function. Apart from some noise, the same compensation is achieved for both, modulation of the second input of the PID controller and current stealing modulation of the master laser.

As shown in Figure 3.9 the derivative part can not create a phase lead outside its own bandwidth. Since there is nothing in the fast path of the loop with a significantly lower bandwidth than the PID controller, the derivative part can not be used to push the servo bump to higher frequencies. The main problem here is that outside its bandwidth the derivative part does not create a phase lead but increases the absolute value of the output amplitude of the controller in comparison to without the derivative part. This results in an increase of the servo bump, which is not desirable. Therefore the derivative part can lead to great improvement of the stabilization when its bandwidth is larger than the bandwidth of the full loop but for this specific feedback loops it is not a useful tool. The PID controllers are therefore used as PI controllers for both stabilizations.

The next step is to optimize the proportional and integral gain to reach the best possible compensation curve. The optimized closed loop compensation curve for the beatnote stabilization as well as the measured noise of the monitoring error output without any PID input are shown in Figure 3.14. Up to roughly 800 Hz the compensation curve is in the same order of magnitude as the noise of the monitoring error output. This means that for frequencies lower than 800 Hz the compensation is better than it can be measured with the monitoring error output of the PID controller. The frequency span where noise is suppressed is close to 1 MHz and the servo bump height is approximately 3 dBm.

After the first feedback loop was optimized, the other had to be optimized. The generated error signals,

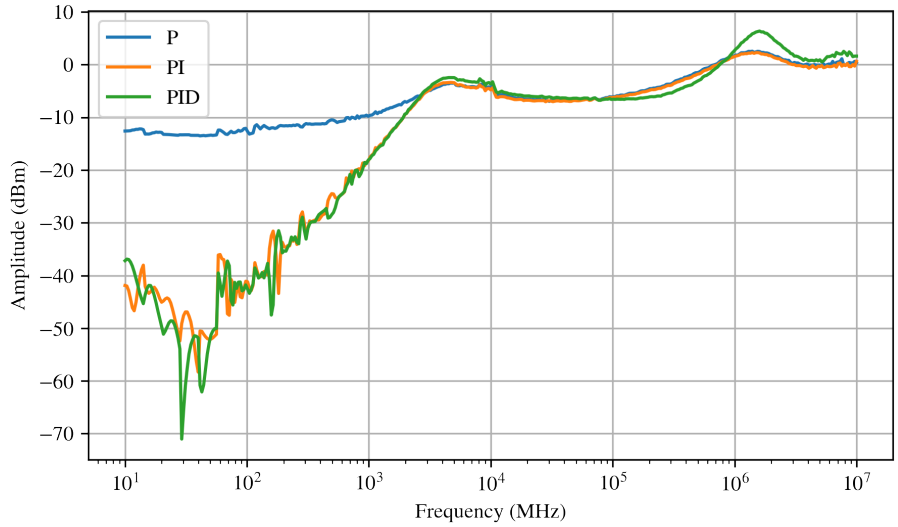

Figure 3.13: Compensation curves with proportional, proportional and integral and proportional, integral and derivative part.

setup shown in Figure 2.7, differ in magnitudes as the error signal to the optical reference has a slope of 29.5 mV/MHz. In comparison, the error signal to the atomic reference has a slope of 0.12 mV/MHz. Stabilization with the atomic reference cannot be achieved with an attenuation of the slow output since the potentiometer ranges to adjust the gains of the PID controller are not wide enough. The problem is that not only the fast feedback path but also the slow feedback path has its servo bump. For the beatnote stabilization, the servo bump of the slow path could be compensated by the fast path due to the attenuation. The attenuation of the slow path negatively impacts the long term stability as it lowers the frequency drift compensation range. The optimized compensation curve for the master laser stabilization as well as a compensation curve with a too high integrator gain are shown in Figure 3.15. The servo bump of the slow path limits the integrator gain as a too high integrator gain leads to an overshoot of the servo bump. Therefore the integrator gain can not be chosen here as high as for the beatnote stabilization. The flat structure at the top of the servo bump for the compensation curve with too high integrator gain in Figure 3.15 is misleading as it does not mean that the change of laser frequencies for disturbing frequencies in this span is the same. The amplitude is here limited by the dip size of the error signal.

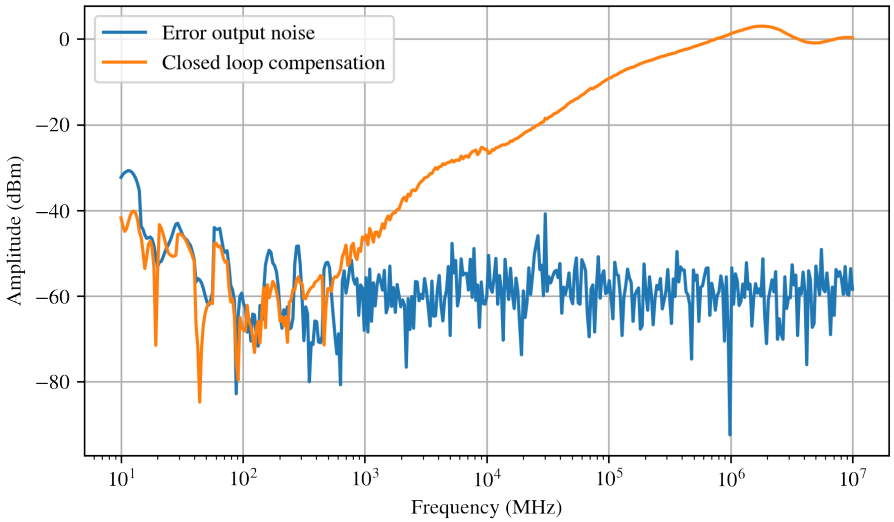

Figure 3.14: Beatnote stabilization optimized compensation curve and error output noise measured with the network analyzer. The compensation curve is the difference between the open loop and closed loop transfer function.

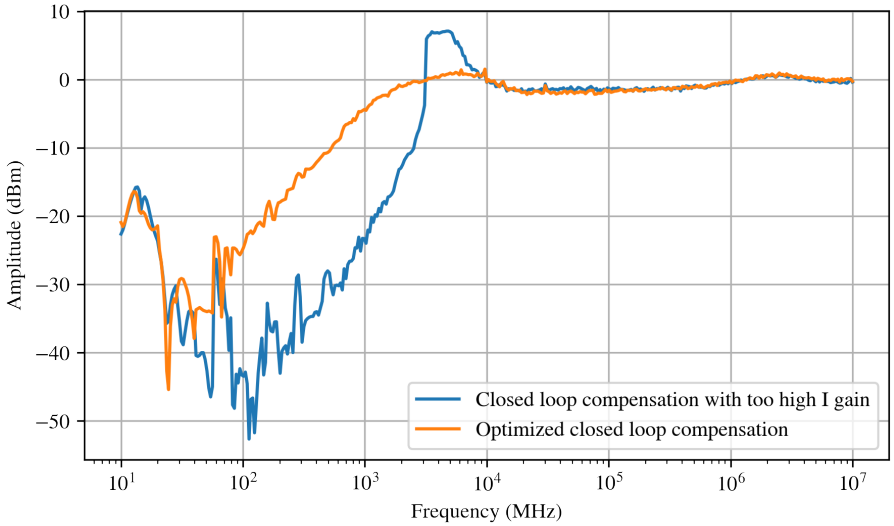

Figure 3.15: Optimized closed loop compensation and closed loop compensation with too high Integrator gain for the stabilization of the master laser. The compensation curve is the difference between the open loop and closed loop transfer function.

3.5 Long term stability

In order for the stabilized lasers to be applied in an experiment, it is important that the stability can be maintained over a longer period of time. Therefore a long term measurement was done by keeping the lasers stabilized overnight. The frequency of the master laser was measured with a wavemeter[2] during this process while the beatnote frequency was measured with the max hold feature of the spectrum analyzer. The max hold feature works by outputting the highest amplitude measured for each frequency that has been reached since the measurement was started.

Only the stabilization of the master laser lasted overnight. As described in section 3.4 the slow output of the PID controller used for the beatnote stabilization has to be attenuated. The consequence is a lower range for the piezo modulation which results in the limit of frequency drift compensation being reached earlier. The long term result of the master laser stabilization is shown in Figure 3.16 as well as the frequency drift for the unstabilized laser in this time period. It shows that the frequency stabilization is highly stable for the first 4.5 hours. After that the frequency slowly starts to drift resulting in an overall frequency drift of roughly 70 MHz in 16 hours. The frequency drift without stabilization is more than eleven times higher. It is possible that this frequency drift is reduced if the integrator gain is increased which can not be done in this configuration as described in section 3.4. Another possibility would be that the power of the laser changes slightly after a longer period of time, which would shift the frequency of the zero crossing of the error signal.

After the overnight beatnote stabilization did not last, the measurement was repeated for a shorter period of time. The result is shown in Figure 3.17. For the first 2.5 hours the beatnote frequency is highly stable as its curve almost overlaps completely with the curve after one hour. The laser frequency only changes a tiny fraction of a MHz in this time period. After three hours the system starts getting unstable as the output value of the PID controller approaches the maximum possible output value which leads to nonlinear effects. After 3.5 hours the system is significantly more unstable and reached laser frequency fluctuations up to 6 MHz. After around 3 hours and 40 minutes the stabilization failed.

The main problem remaining is that the integrator gain is limited by the servo bump of the slow feedback path unless it is attenuated. However, the attenuation reduces the piezo span of frequency drift compensation and therefore the time span of the stabilization. To solve this the fast output can be amplified. This could be done by using a non-inverted amplifier [17] (p.328). A potentiometer could easily be implemented to control the amplification value which would be extremely practical since the current stealing response changes for different current supplies as described in section 3.1. This provides an additional parameter with which adjustments can easily be made if the lasers should be used for another application where another laser frequency, and therefore also another current supply amount, is needed. Another approach would be to use different PID controllers for the fast and the slow feedback path. This way the proportional, integral and derivative gain can be adjusted for each feedback path separately which would add enough parameters to find a setting so that the fast feedback path compensates the servo bump of the slow feedback path without attenuating the slow PID output. With both of these approaches it should be possible to achieve a closed loop compensation curve in frequency domain as with the beatnote stabilization in Figure 3.14 while simultaneously making the

[2] High Finesse WS7 - 1761

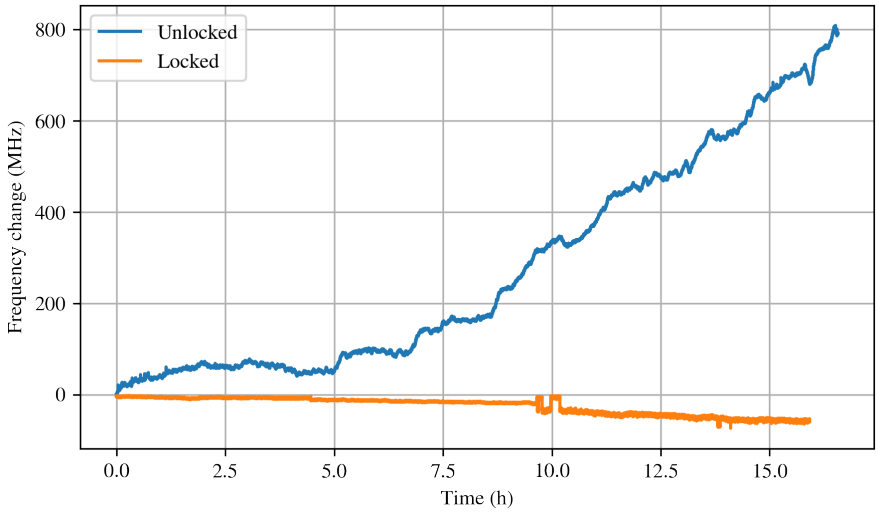

Figure 3.16: Long term measurement of the frequency drift with and without frequency stabilization to the atomic reference. The measurement was taken with a wavemeter.

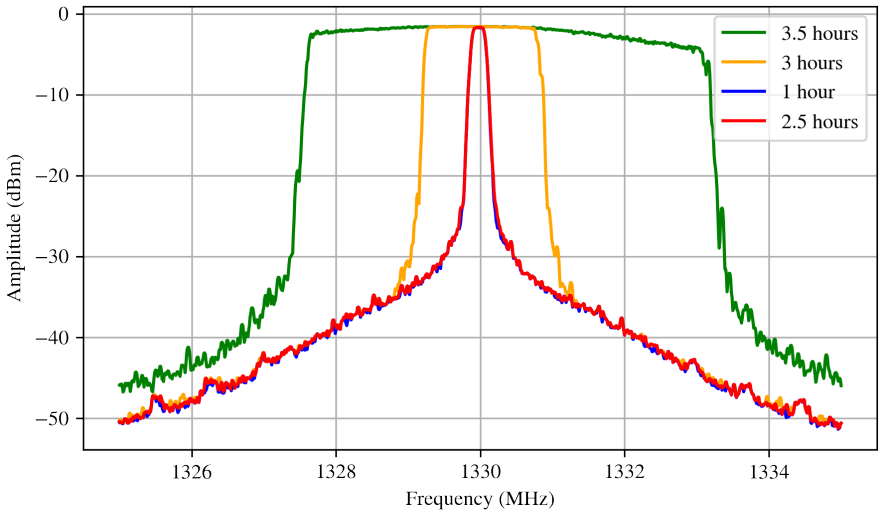

Figure 3.17: Max hold measurement with the spectrum analyzer of the beatnote stabilization after different intervals of time.

stabilization last for more than 16 hours.

CHAPTER 4

Conclusion and Outlook

For this thesis feedback loops for the frequency stabilization of two home-built interference filter lasers were constructed. They were previously refurbished to 780 nm to use them for cold atom experiments with rubidium. The goal was to stabilize one laser to an atomic reference and stabilize the other laser relative to the first laser.

First of all, error signals had to be generated for both stabilizations. For the first laser, the hyperfine structure transition $F = 2 \rightarrow F = 2'$ of the D_2-line in Rubidium was chosen as a reference. For this purpose, Doppler-free saturated spectroscopy was set up and used to generate an error signal. The first laser was used as a reference for the second laser. For this purpose, both laser beams were overlapped with the same polarization, and the beatnote frequency was detected with a photodiode. A delay line box was used to generate a phase shift dependent on the beatnote frequency, resulting in a cosine-shaped error signal. Given that the delay line length is a parameter that controls the error signal slope independent of the amount of light used leads to significantly different slopes as the amount of light used for the spectroscopy should be as low as possible so that most of the light is available for applications with the stabilized laser. For the error signal creation with Doppler-free saturated absorption spectroscopy the error signal slope reached 0.12 mV/MHz for a low amount of light used whereas the error signal slope generated by the delay line box reached 29.5 mV/MHz with a delay line of roughly four meters.

After the two error signals were created, the feedback loop was optimized through several implementations. Since the piezo modulation can only be used for low-frequency and drift compensation, a current stealing modulation was implemented as a safe way of modulating the laser diode current and thereby suppressing high-frequency noise. A PID controller was implemented as a control algorithm that outputs feedback with a proportional, integral, and derivative component. Due to the limited bandwidth of the PID controller, the derivative part primarily amplifies the servo bump. Therefore the PID controller is used as a PI controller in both feedback loops. The controller has two outputs which are denoted as slow and fast output. A lowpass filter is implemented in the slow output, which is used for piezo modulation. This filter is needed to prevent the piezo from driving mechanical resonances in the 10 kHz regime. The fast output is used for current stealing modulation. To push the servo bump to higher frequencies, a phase advancer was implemented into this loop, which utilizes the frequency-dependent capacitive resistance of a capacitor.

Both feedback paths have their own servo bump. The fast feedback path was not able to compensate for the servo bump of the slow feedback path. This problem can be solved by attenuating the fast output which led to a significantly better short term stability and a compensation bandwidth of roughly 1 MHz. However, this solution negatively affects the long term stability. The beatnote stabilization was done with attenuation of the slow output and lasted roughly 3.5 hours. In comparison, the other stabilization was done without this attenuation and lasted more than 16 hours.

The main goal of this thesis to realize a frequency stabilization to an atomic and an optical reference was achieved. However, this feedback loops can still be improved. First of all the compensation bandwidth of the beatnote lock has to be achieved for both stabilizations without an attenuation of the slow output, making it last for more than 16 hours. This could be realized by implementing an amplifier for the fast feedback path or by using two different PID controllers for the piezo and current stealing modulation, allowing to adjust the gains for both feedback paths separately.

The next thing that can be done is to increase the bandwidth of compensation even further. Therefore another current modulation version could be implemented to give the modulation signal through a resistor and a capacitor directly to the laser diode, resulting in higher bandwidth current modulation. However, for this to lead to an improvement, the PID controller must be exchanged and replaced by another one with a higher bandwidth. One possible option would be the D2-125 Reconfigurable Laser Servo, which is owned by the Nonlinear Quantum Optics Group and whose bandwidth is larger than 10 MHz [22]. This PID controller could also lead to a useful application of the derivative part due to its higher bandwidth.

Bibliography

[1] T. Maiman, *Stimulated Optical Radiation in Ruby*, Nature **187** (1960) 493.

[2] C. Wiemann and L. Hollberg, *Using diode lasers for atomic physics*, Review of Scientific Instruments **62** (1991) 1.

[3] H. Metcalf and P. van der Straten, *Laser cooling and trapping of atoms*, Journal of the Optical Society of America B **20** (2003) 887.

[4] L. Johnson, H. Majeed and B. Varcoe, *A three-step laser stabilization scheme for excitation to Rydberg levels in 85Rb*, Applied Physics B Lasers and Optics **106** (2011) 257.

[5] S. Schmidt-Eberle, "Phase and Frequency Locking of Diode Lasers".

[6] H. Buss, *Refurbishing Interference Filter External Cavity Diode Lasers for Cold Atom Experiments*, Bachelor thesis, 2024.

[7] D. Steck, "Rubidium 87 D Line Data (revision 2.3.3)", 2024.

[8] J. Boyd and T. Lahaye, *A basic introduction to ultrastable optical cavities for laser stabilization*, American Journal of Physics **92** (2024) 50.

[9] E. Black, *An introduction to Pound–Drever–Hall laser frequency stabilization*, American Journal of Physics **69** (2001) 79.

[10] M. Fleming and A. Mooradian, *Spectral characteristics of external-cavity controlled semiconductor lasers*, IEEE Journal of Quantum Electronics **17** (1981) 44.

[11] P. Zorabedian, "8 - Tunable External-Cavity Semiconductor Lasers", *Tunable Lasers Handbook*, ed. by F. Duarte, Optics and Photonics, San Diego: Academic Press, 1995 349.

[12] B. T. H. Varcoe et al., *Long term laser frequency control for applications in atomic physics*, Measurement Science and Technology **11** (2000) 111.

[13] D. W. Preston, *Doppler-free saturated absorption: Laser spectroscopy*, American Journal of Physics **64** (1996) 1432.

[14] J. R. De Laeter et al., *Atomic weights of the elements. Review 2000 (IUPAC Technical Report)*, Pure and Applied Chemistry **75** (2003) 683.

[15] U. Schünemann, H. Engler, R. Grimm, M. Weidemüller and M. Zielonkowski, *Simple scheme for tunable frequency offset locking of two lasers*, Review of Scientific Instruments **70** (1999) 242.

[16] J. Appel, A. McRae and A. Lvovsky,
A versatile digital GHz phase lock for external cavity diode lasers,
Measurement Science and Technology **20** (2009) 1.

[17] S. Gift and B. Maundy, *Electronic Circuit Design and Application*, Second edition,
Gewerbestrasse 11, 6330 Cham, Switzerland: Springer Nature Switzerland, 2022,
ISBN: 978-3-030-79374-6.

[18] J. Bechhoefer, *Feedback for physicists: A tutorial essay on control*,
Reviews of Modern Physics **77** (2005) 783.

[19] M. E. and V. Valkenburg, *Analog Filter Design*, International edition,
383 Madison Avenue, NY: CBS College Publishing, 1982, ISBN: 4-8338-0091-3.

[20] R. Fox, C. Oates and L. Hollberg, *Stabilizing diode lasers to high-finesse cavities*,
Experimental Methods in The Physical Sciences **40** (2003) 1.

[21] N. Nise, *Control Systems Engineering*, Seventh edition,
111 River Street, Hoboken, NJ: John Wiley and Sons, 2015, ISBN: 978-1-118-80063-8.

[22] Vescent, *Reconfigurable Laser Servo Model No. D2-125*, 2021,
URL: https://www.vescent.com/manuals/doku.php?id=d2:laser_servo (visited on
07/08/2024).

APPENDIX A

Appendix

A.1 Figures

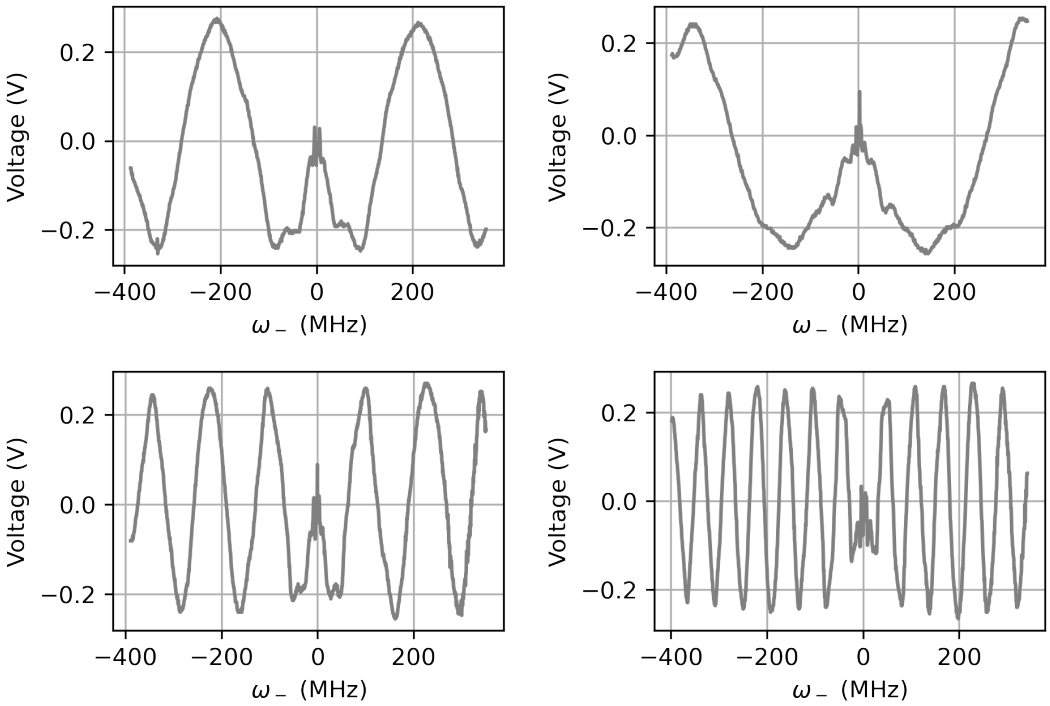

Figure A.1: Measured error signals for different delay line lengths around $\omega_- = 0$ (top left ($l = 58.0 \pm 1.0$) cm, top right ($l = 98.5 \pm 1.5$) cm, bottom left ($l = 197.5 \pm 3.5$) cm, and bottom right $l = (397.5 \pm 4.5)$ cm). The expected cosine relation can be seen as well as disturbances at $\omega_- \approx 0$ which can be explained by the time dependent term in equation 2.8. The cosine frequency gets higher for longer delay lines. The measurement was done by giving a ramp signal to the piezo modulation while simultaneously measuring the beatnote frequency with a spectrum analyzer.

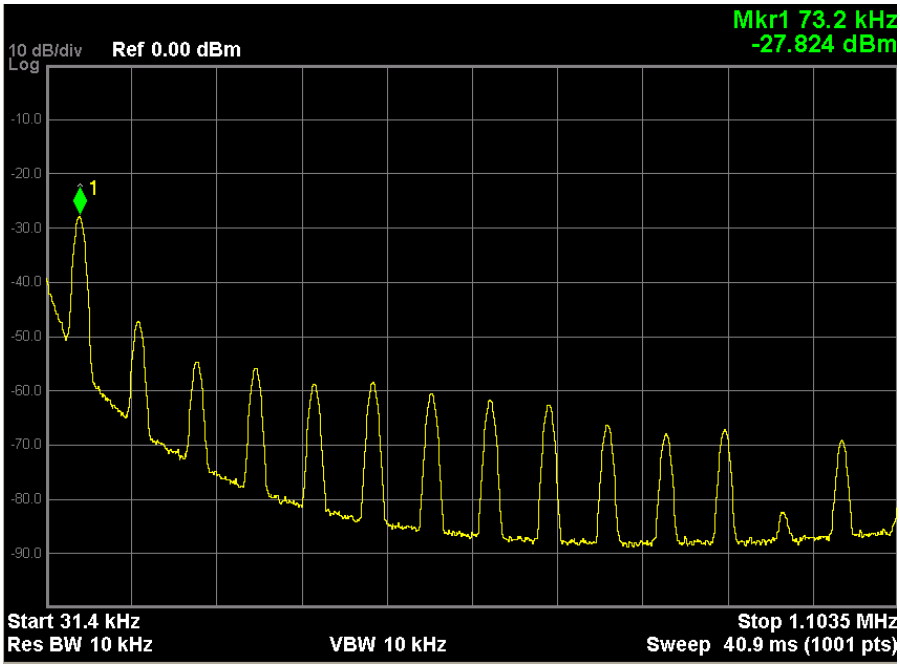

Figure A.2: The delay line box input was given to the piezo elements of the laser while simultaneously observing a part of the delay line box input with the spectrum analyzer. The 73 kHz resonance of the piezo elements can be seen.

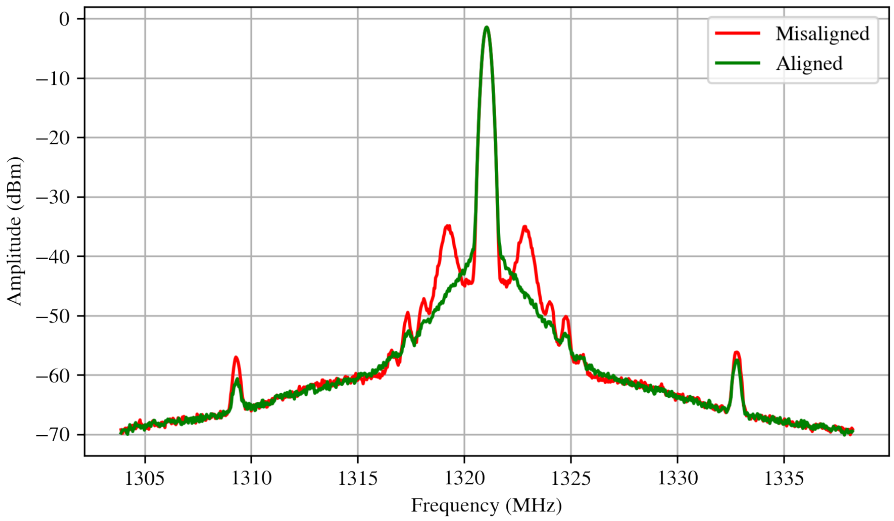

Figure A.3: Beatnote signal measured with the spectrum analyzer and averaged over 100 scans with a aligned and a totally misaligned PID parameters. It shows that servo bumps can also be observed in the frequency domain of the beatnote signal.

A.2 Tables

Delay line length in m	Slope in mV/MHz	Capture range in MHz
0.58 ± 0.01	4.11 ± 0.11	374 ± 3
0.985 ± 0.015	7.08 ± 0.30	230 ± 3
1.975 ± 0.035	14.92 ± 0.57	125 ± 3
3.975 ± 0.045	29.5 ± 1.3	56 ± 3

Table A.1: Extracted slopes and capture ranges for different delay lines.

Acknowledgements

I want to thank Prof. Hofferberth for giving me the opportunity to write my thesis in his group and Prof. Wang for being my second appraiser. I want to thank them both for inspiring me with their great Quantum Optics lecture to write my thesis in this field.

It is important to me to express my thanks to Lukas for his supervision in the lab and his great guidance throughout the entire project. His engagement was essential to the success of the project. I also want to thank Nina for her help whenever I had questions and her help in soldering the parts for the current stealing modulation into the laser board. I want to thank Wolfgang for the interesting talks about laser stabilization and his ideas and advice which led to great improvements in the project.

I would like to thank Lukas, Nina, and Daniil for proofreading my thesis and giving me valuable feedback. I want to thank the entire NQO group for making me feel welcome and for the great group atmosphere. Finally, I would like to thank my family for their support.